ENGINOM | Engineering Innovations

Available online at www.enginom.org
ENGINOM in Engineering Innovations
(E-ISSN: xxxx-xxxx; ISSN: xxxx-xxxx)
Vol. 1, No. 01, March, 2026

Radiation Aspects and Performance of Geo-polymerized Zeolite Concrete

Article,

Abd Al-Kader A. Al Sayed [1,*], **Amr Abdelkhalik** [1,2]

1 Department of Civil Engineering, College of Engineering and Information Technology, Onaizah Colleges, Qassim, Saudi Arabia;
2 Civil Engineering Department, Badr University in Cairo, Cairo, Egypt; amr_civileng@oc.edu.sa,
* **Corresponding author**: Abd Al-Kader A. Al Sayed,

Academic Editor:
Essam Mohammed

Submission: 22 April 2026
Revision: 27 April 2026
Acceptance: 30 April 2026

Citation: To be added by editorial staff during production.

Abstract

A series of concrete mixtures was prepared by substituting cement with zeolite at replacement levels of 0, 25, 50, 75 and 100 wt%. The study examined the mechanical properties, corrosion behavior of embedded steel reinforcement, and various nuclear radiation attenuation parameters for five concrete mixes. Corrosion performance was assessed through multiple electrochemical methods and optical microscopy. Furthermore, three neutron energy levels and nine gamma-ray energy lines (ranging from 121.78 to 1407.92 keV) were employed to determine the macroscopic neutron cross-sections (Σ, cm^{-1}) and the mass attenuation coefficients (σ, cm^2/g) for gamma rays within the concrete specimens. The findings indicated that both the mechanical strength of the concrete and the corrosion resistance of the embedded steel improved with the addition of zeolite up to 50 wt.%. For the mass attenuation coefficients corresponding to most of the investigated gamma-ray energies, the optimal zeolite content was found to be 50 wt.%.

Keywords: Zeolite; Radiation; Geopolymer; Alkaline; Sodium hydroxide; Activators.

1. Introduction

Nuclear technology is now essential for many crucial applications that gauge a country's level of development and civilization. Identification and treatment of diseases, food safety and quality, water desalination, pollution control, manufacturing processes, electricity generation, archaeology, military uses, etc. are examples of typical applications [1], [2]. Nuclear technology has many benefits, but it mostly relies on radioactive isotopes [3]. Conversely, due to its low cost, great strength, sufficient durability, ease of manufacturing on-site, and substantial radiation shielding, concrete is the best option for radiation protection [4], [5]. The primary traditional binding agent used in concrete is Portland cement [6], [7]. Unfortunately, as cement use increased, economic and environmental issues started to surface [8]. One of the primary businesses that has a significant impact on the problem of global warming is the manufacturing of cement, which accounts for 5–7% of all greenhouse gas emissions [5], [9].

A number of factors, including glass fineness, curing temperature, concentration of alkali-activated solution, and aluminosilicate precursor composition, influence the physico-mechanical characteristics of geopolymer-containing glass waste [10], [11]. Glass waste's pozzolanic activity was shallow over a particle size distribution threshold of 75 µm [6], [9], [12]. Glass waste with a particle size distribution of less than 38 µm showed a discernible pozzolanic activity, but glass trash with a particle size distribution between 38 and 75 µm showed little activity or a loss [13], [14], [15].

A promising substitute for materials like glass, modified plastics, or red mud, which are presently the subject of extensive research, is geopolymers [16]. Aluminosilicate precursors

are polycondensed at low temperatures in a strongly alkaline solution to create these inorganic compounds [17]. They are categorized as alkali-activated materials in which the aluminosilicate binding phase forms an amorphous to semicrystalline three-dimensional network of linked SiO_4 and AlO_4 tetrahedra [18], [19]. Unlike the chain-like calcium silicate hydrates seen in conventional cements, this network resembles a pseudo-zeolite structure [10]. Calcined materials like metakaolin or different waste materials like fly ash from burning coal, rising husk ash, straw ash, bottom ash, red mud, or waste red brick powder are examples of aluminosilicate precursors [20], [21], [22].

Alumino-silicate polymerization takes place at ambient or low temperatures and is started under alkaline conditions at very high pH. These materials' primarily non-crystalline, three-dimensional, interconnecting structure is produced by a multi-step geo-polymerization reaction. Alumino-silicates are dissolved in a highly alkaline solution to produce free SiO_4 and AlO_4 hydrated species. Diffusion of dissolved Al and Si complexes from the particle surface to the interparticle space causes the formation of a gel phase, which is then hardened by condensation reactions to form the geopolymer, which has amorphous to semi-crystalline structures akin to zeolites. In order to create a homogeneous powder layer that will form the whole print bed and be free of flaws that would otherwise appear in the final printed item, raw material powder qualities (such as particle size and distribution, density, flowability, packing, etc.) are crucial. The powder must have adequate flowability so that the printer can deposit a uniform layer of particles without creating macro-defects, which occur when a dry fine powder is spread because of strong interparticle forces that tend to bind the particles together and impede their flow. Starting powders must therefore be large enough (usually more than 20 μm) and ideally spherical.

In the current investigation, a system comprising sand particles and a solid reactive component (Zeolite) was sprayed with a highly alkaline solution over a powder bed. A sodium-based solution was the type utilized. In order to gain a better understanding of the processes involved and the mechanism of geopolymer gel formation up to the full hardening of printed parts, a comparison with water was also conducted. To precisely describe the initial powder at various scales, from the granule to the powder bed as deposited in the printer, non-destructive volume observations were specifically conducted.

1.1. Research Significance

This study holds significant importance in advancing sustainable construction materials while addressing critical performance demands in both structural and radiation-sensitive applications. The investigation of geo-polymerized zeolite concrete provides a novel approach to reducing dependence on Ordinary Portland Cement, thereby lowering carbon emissions and promoting environmentally responsible construction practices. By integrating naturally occurring zeolite with geopolymer technology, this research explores the dual benefit of enhancing mechanical performance and improving durability, particularly in aggressive environments where conventional concrete may be vulnerable to degradation. Moreover, the evaluation of radiation attenuation properties introduces an added dimension of functionality, positioning this material as a promising candidate for specialized infrastructure such as medical facilities, nuclear power plants, and radiation shielding structures. The study contributes to bridging the gap between sustainable material development and high-performance engineering requirements by demonstrating how alternative binders can meet both structural and protective criteria. In addition, the findings provide valuable insights into the microstructural behavior and interaction mechanisms responsible for improved performance, supporting future optimization and large-scale implementation. Ultimately, this research not only contributes to the body of knowledge in geopolymer and zeolite-based materials but also offers practical implications for engineers, designers, and policymakers seeking

innovative solutions that align with global sustainability goals and advanced engineering applications.

2. Methodology

2.1 Material properties

The materials utilized in this study included Ground Granulated Blast Furnace Slag (GGBFS), Ordinary Portland Cement (OPC), and both fine and coarse aggregates. The GGBFS employed in the experimental program was obtained from the Egyptian Iron and Steel Company located in Helwan, Egypt, and represented an air-cooled byproduct generated during iron and steel manufacturing processes. The Ground Granulated Blast Furnace Slag (GGBFS) used in this study exhibited a chemical composition rich in calcium and silica compounds, making it suitable for use as a supplementary cementitious material in concrete applications. As presented in the chemical analysis, the slag mainly consisted of calcium oxide (CaO) at 36.8% and silicon dioxide (SiO_2) at 31%, in addition to aluminum oxide (Al_2O_3) at 8.3% and magnesium oxide (MgO) at 4.31%. Minor quantities of iron oxide (Fe_2O_3), sulfur trioxide (SO_3), sodium oxide (Na_2O), potassium oxide (K_2O), titanium dioxide (TiO_2), and phosphorus pentoxide (P_2O_5) were also detected. Furthermore, the loss on ignition (L.O.I.) value was relatively low at 2.7%, indicating limited unburned or volatile constituents. The total oxide content reached approximately 97.91%, reflecting the high purity and stability of the slag material used throughout the experimental investigation.

Table 1. Chemical composition of Zeolite

Oxides content	SiO_2	Al_2O_3	Fe_2O_3	CaO	MgO	Na_2O_3	K_2O	SO_3	TiO_2	LOI
Zeolite	31	8.3	2.98	36.8	4.31	0.64	0.45	3.34	0.21	2.7

The chemical composition of the slag is provided in Table 2 of the original document. In addition, a commercially available Ordinary Portland Cement classified as CEM I 42.5 N and conforming to the Egyptian Standard Specification ESS 2421/2007 was used as the primary cementitious material. The physical, chemical, and mechanical properties of the cement are summarized in Table 1 of the original document. Regarding aggregates, the fine aggregate consisted of natural siliceous sand characterized by a fineness modulus of 2.66 and a specific gravity of 2.67, while the coarse aggregate was crushed dolomite with a maximum nominal aggregate size of 18 mm, a specific gravity of 2.64, and a crushing modulus of approximately 23%, making it suitable for concrete production and mechanical performance evaluation.

2.2 Specimen preparation and curing

A tilting drum mixer was used to prepare the concrete mixtures. First, the weighed coarse and fine aggregates were placed into the mixer and blended for 30 seconds to achieve a uniform mix. The cementitious materials were then added and mixed for two minutes. Water was introduced gradually, and mixing continued for another two minutes, followed by an additional three minutes of mixing. Under laboratory conditions, six 150 mm cubes and six cylinders measuring 150 × 300 mm were cast and compacted using a vibrating rod. For corrosion testing, steel bars were cleaned with ethanol, dried, and then embedded centrally in the 150 mm cube molds with a concrete cover of 25 mm. After casting, all specimens were covered with plastic sheeting and left in the lab for 24 hours. They were then demolded and submerged in water for 28 days. Additionally, one of the prepared cylinders was cut into

sections with thicknesses ranging from 3.5 mm to 20 cm for nuclear radiation (gamma rays and neutrons) measurements. Tap water is acceptable as mixing water, but distilled water—as used in the current experimental program—is preferred to avoid any potential chemical reactions.

2.3 Specimen preparation and curing

The consistency and workability of fresh concrete are critical parameters that govern the ease of mixing, placement, compaction, and finishing, ultimately affecting the strength and durability of the hardened material. Workability is not a single fundamental property but a combination of rheological characteristics, including slump, flowability, stability, and cohesiveness. While the slump cone test, as mentioned in the source document, is the most common empirical method for measuring workability, it is widely acknowledged that it has significant limitations; two concretes with identical slump can exhibit vastly different workability behaviors during handling and placement. The limitations of the slump test have led to a paradigm shift towards rheological characterization, which describes concrete flow using two fundamental parameters: yield stress and plastic viscosity. These parameters are considered a more material science-based approach to characterize fresh concrete, allowing for a better understanding of its performance.

2.4 Mechanical tests

Mechanical testing is fundamental for evaluating the structural performance and load-bearing capacity of concrete. As noted in the source document, compressive strength tests are routinely performed on cube or cylinder specimens at various curing ages (e.g., 3, 7, and 28 days). The uniaxial compressive strength is a primary design parameter, often used as an indicator of overall concrete quality. For tensile strength, the source mentions tests on cured cylinders. The direct measurement of tensile strength is challenging due to difficulties in perfectly aligning the specimen and avoiding stress concentrations. Consequently, indirect methods are more common. The splitting tensile test (or Brazilian test) is a widely accepted standard method for estimating the tensile strength of concrete. However, a recent comprehensive review indicates that indirect methods like the splitting test generally overpredict the true tensile strength compared to direct tension tests, with factors like concrete grade, specimen shape and size, and casting direction significantly influencing the results

2.5 Electrochemical corrosion tests

Electrochemical techniques are indispensable, non-destructive methods for assessing the corrosion state of steel reinforcement in concrete. Steel corrosion is the primary cause of premature degradation and failure in reinforced concrete structures. The source document describes the use of a Potentiostat/Galvanostat for conducting open-circuit potential (OCP) monitoring, potentiodynamic polarization, and cyclic potentiodynamic tests within a three-electrode cell. These techniques are part of a broader suite of electrochemical methods. Potentiostatic transients can be recorded in a short time (approx. 30 seconds), making them highly efficient. In contrast, advanced methods like AC impedance and galvanostatic transients may require much longer measurement periods (up to several hours) to obtain comprehensive data on the steel-concrete interface. Each technique offers unique advantages; for instance, coulostatically induced transients provide a very short perturbation, minimizing changes to the steel's corrosion state during measurement

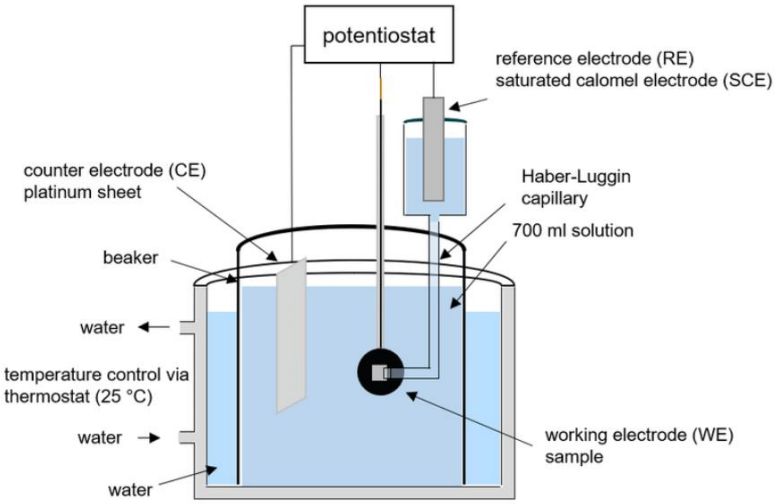

Figure 1. Electrochemical corrosion measuring experiment setup

2.6 Microstructure Analysis

The macro-performance of concrete, including its strength, durability, and permeability, is fundamentally governed by its microstructure. Advanced analytical instruments are therefore essential for understanding and optimizing concrete formulations. The source document mentions the use of X-ray diffraction (XRD) and scanning electron microscopy (SEM) to investigate the structure of concrete with and without blast furnace slag. XRD is a powerful tool for identifying and quantifying the crystalline phases present in cementitious materials, such as alite, belite, and calcium silicate hydrate (C-S-H) gel, providing insights into hydration reactions and phase stability. Simultaneously, SEM provides high-resolution imaging of the material's external morphology, revealing critical microstructural features like hydration products, pore structure, micro-cracks, and the interfacial transition zone (ITZ). When coupled with energy-dispersive X-ray spectroscopy (EDS), SEM can also provide localized elemental composition analysis

2.7 Calculations and measurements of neutrons and gamma rays

Concrete is a versatile and cost-effective material used extensively for radiation shielding in nuclear facilities, owing to its ability to attenuate both gamma rays and neutrons. The source document outlines an experimental setup using an Am-Be neutron source, a BF_3 detector, and various filters to measure neutron transmission and calculate macroscopic cross-sections. Similarly, for gamma rays, the document describes measuring the linear attenuation coefficient (μ) from transmission experiments using sources like Eu-152, Cs-137, and Co-60. The hydrogen content within the concrete is critical for effectively attenuating fast neutrons through elastic scattering, while the high density of concrete (often enhanced with heavy aggregates like barite, magnetite, or steel slag) is essential for gamma-ray attenuation, which occurs primarily via photoelectric absorption and Compton scattering. The mass attenuation coefficient (μ/ρ) is a density-independent parameter, allowing for a more fundamental comparison of a material's shielding efficacy against gamma rays across different compositions

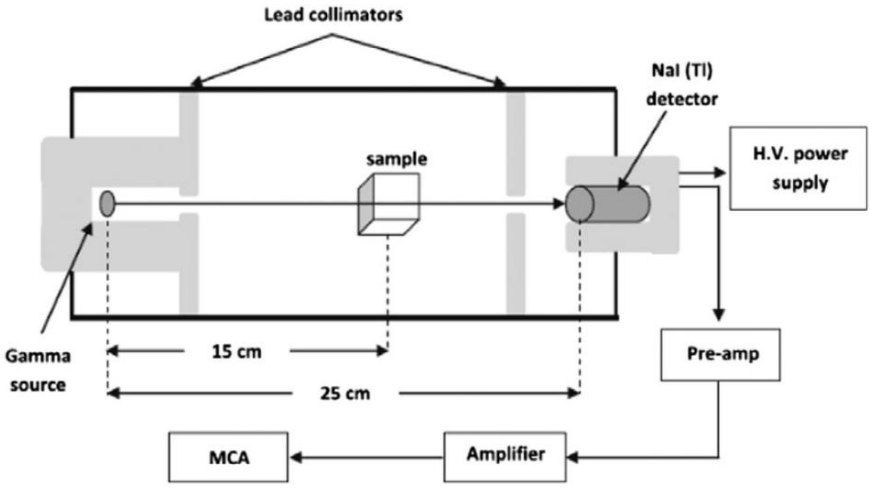

Figure 2. Schematic diagram of Neutron spectrometer

Gamma-ray attenuation measurements are commonly used to evaluate the radiation shielding capability of construction and engineering materials. The fundamental principle governing gamma-ray attenuation is the Lambert–Beer law, expressed as [Equation 1] where I_0 represents the initial radiation intensity, I is the transmitted intensity after passing through the shielding material, μ is the linear attenuation coefficient, and x is the material thickness. This equation describes the exponential reduction in gamma-ray intensity as radiation penetrates matter.

The linear attenuation coefficient (μ) is one of the most important shielding parameters because it indicates the effectiveness of a material in absorbing or scattering gamma photons. Since shielding efficiency is also influenced by material density, the mass attenuation coefficient ($\mu_m=\mu/\rho$) is used to normalize attenuation performance with respect to density. Additional important parameters include the Half-Value Layer (HVL) and Tenth-Value Layer (TVL), which represent the thickness required to reduce radiation intensity to 50% and 10% of its original value, respectively. These parameters are essential for practical shielding design in nuclear facilities and medical radiation rooms. The Mean Free Path (MFP) expresses the average distance traveled by photons before interaction occurs inside the material, while the Radiation Protection Efficiency (RPE) and Transmission Factor (TF) quantify the shielding effectiveness and transmitted radiation percentage. In broad beam geometries, the build-up factor is included to account for scattered photons that contribute to the measured intensity. These equations collectively provide a comprehensive framework for evaluating gamma-ray shielding behavior and comparing the radiation attenuation performance of various concrete and geopolymer materials.

$$I = I_0 e^{-\sum \mu^x} \quad (1)$$

Neutron attenuation calculations are essential for assessing the ability of shielding materials to reduce neutron radiation, particularly in nuclear reactors, radiation laboratories, and medical facilities. Unlike gamma rays, neutrons interact primarily through nuclear collisions rather than electromagnetic interactions, making their shielding behavior more complex. The attenuation of neutron intensity is commonly described by [Equation 1], where $\sum R$ is the macroscopic removal cross-section and represents the probability of neutron removal from the incident beam through scattering or absorption processes. The macroscopic removal cross-section depends on the material composition, density, and elemental constituents and is calculated using the summation of the partial contributions of each material component. For heterogeneous materials such as concrete, the fast neutron removal cross-section

equation incorporates the density and weight fraction of each constituent to estimate the overall neutron shielding capability. These calculations are particularly important because materials containing hydrogen-rich compounds or heavy elements often exhibit superior neutron attenuation performance. Additional equations, such as Radiation Protection Efficiency (RPE) and neutron transmission factors, are used to quantify the percentage reduction in neutron intensity after penetration through the shielding material. Detector efficiency equations are also critical in neutron and gamma-ray measurements because they relate the recorded count rate to the actual radiation emitted by the source. Instruments such as helium-3 detectors, BF_3 counters, scintillation detectors, and gamma spectrometers rely on these equations to accurately evaluate radiation flux and attenuation characteristics. Together, these neutron-related equations provide a scientific basis for designing and optimizing advanced radiation shielding materials, including geopolymer concrete and sustainable construction composites intended for nuclear and radiation protection applications.

3. Methodology

3.1 Fresh concrete

The workability of fresh concrete, as measured by the slump test, decreased with increasing slag content. The concrete containing slag as a fine aggregate showed reduced fluidity. This behavior is likely due to the rough texture and high-water absorption characteristics of the slag particles, which absorb a portion of the mixing water, thereby reducing the free water content available for lubrication and flow.

The provided document notes that “the slump test values were decreased with increasing slag content in concrete. This behavior was probably due to the rough texture and high-water absorption of slag particles, leading to low fluidity.”

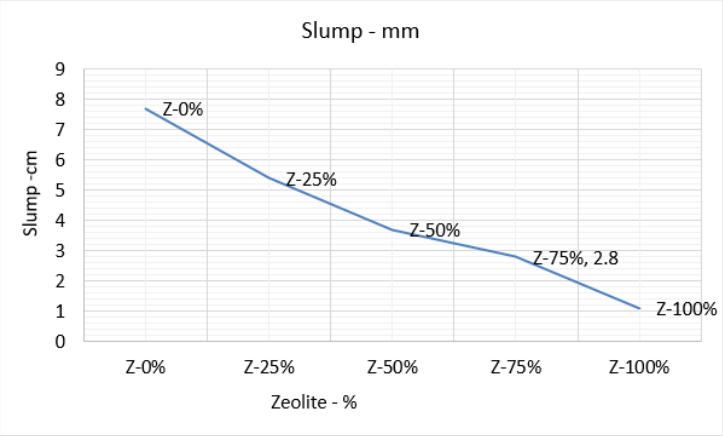

Figure 3. Zeolite's impact on slump value

3.2 XRD Diffraction Patterns

X-ray diffraction (XRD) analysis revealed that the substitution of cement with slag promotes a pozzolanic reaction. In the presence of water, the amorphous silica and alumina in the slag chemically react with the calcium hydroxide (portlandite, $Ca(OH)_2$) liberated during cement hydration. This reaction consumes the portlandite and produces additional calcium-silicate-hydrate (C-S-H) gel, which is the primary binding phase responsible for strength in concrete.

Document Observations:

The document states, “the peaks of portlandite (CH) decreased while the peaks of C-S-H markedly increased with increasing slag content. This behavior was due to the pozzolanic

reaction of slag with the liberated lime, which forms additional amount of C-S-H." It also noted a decrease in $CaCO_3$ peaks, attributed to a lower portlandite content.

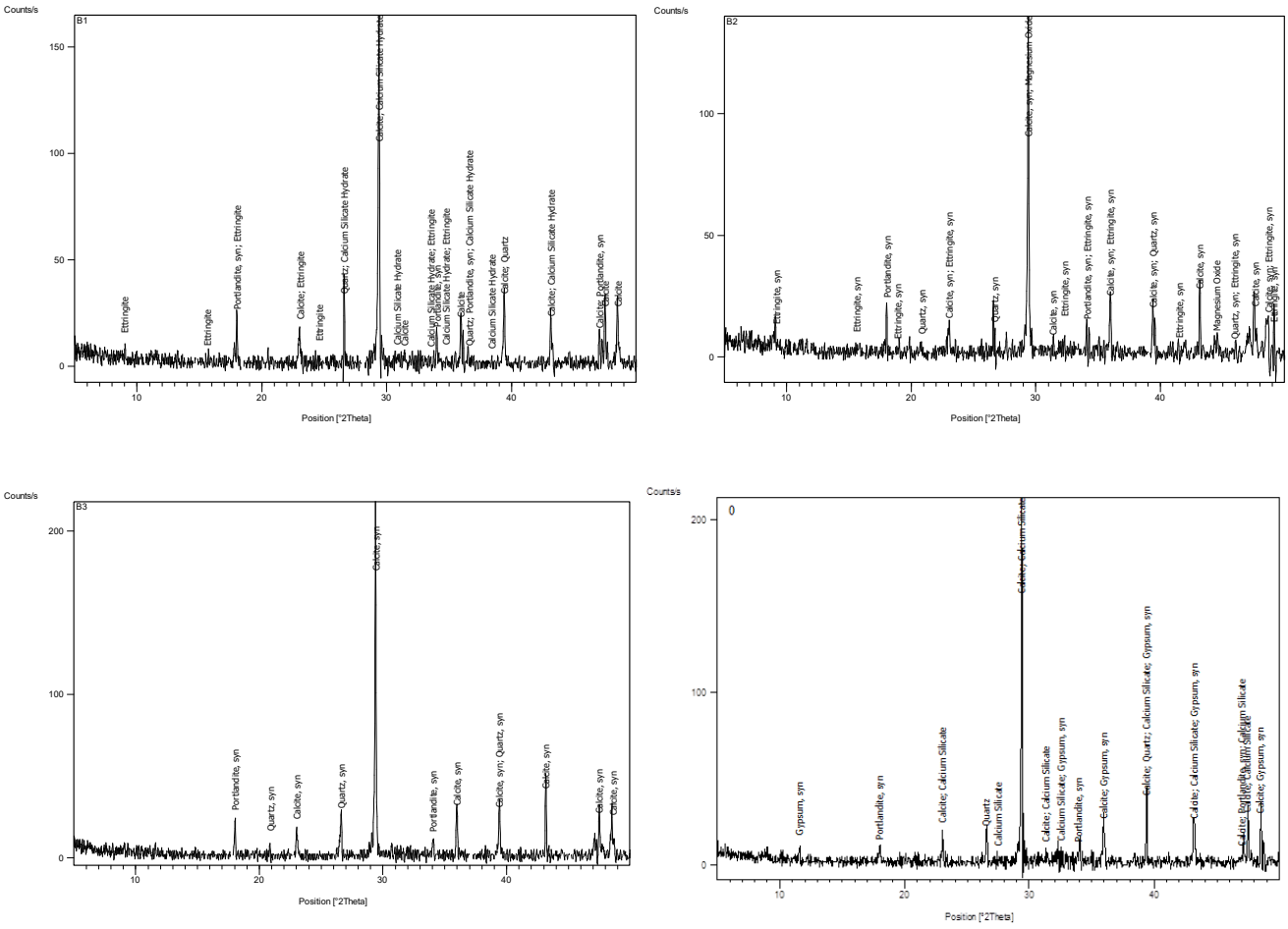

Figure 3. Schematic diagram of Neutron spectrometer

3.3 Compressive Strength

Compressive strength increased with curing time for all mixes, but the 28-day strength improved significantly (by 16-17%) with slag replacement up to 10 wt.%. This is due to the pozzolanic reaction of slag with lime, producing more C-S-H gel, which fills pores and densifies the matrix. However, a replacement level of 15 wt.% or higher caused a slight decrease in strength (approximately 10%), though it remained above the control level. This reduction is attributed to a decrease in workability, leading to increased voids.

The document indicates that "the compressive strength increased by adding slag up to 10 wt.% replacements. Beyond this value, the compressive strength decreased, but still more than the control specimen."

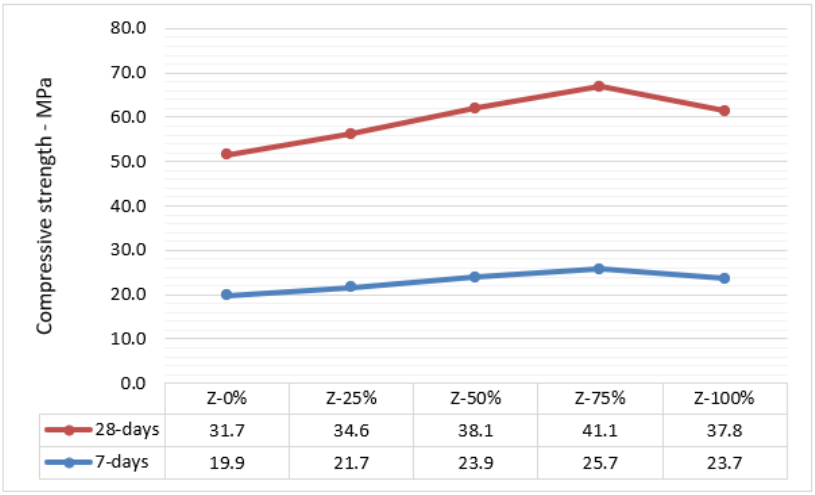

Figure 5. Zeolite's impact on slump value

3.4 Splitting Tensile Strength

The splitting tensile strength followed a trend similar to that of compressive strength. All concrete mixes containing slag exhibited higher tensile strength than the control mix. The optimal performance was again observed at a 10 wt.% cement replacement level. Beyond this point, the tensile strength tends to decrease, though it typically remains higher than the control.

The document notes that "all slag mixes have gained higher split tensile strength than that of the control mix. However, beyond 10 wt.% replacement the tensile strength decreases, but still more than the control mix. The trend was similar to the trend of compressive strength development of concrete."

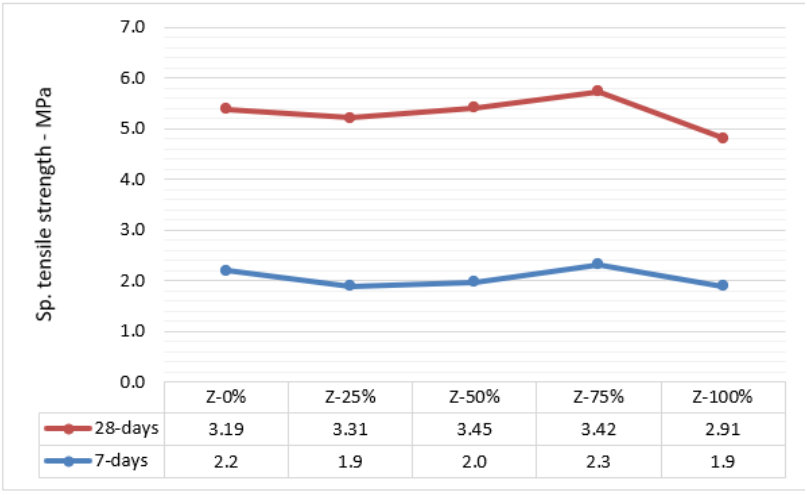

Figure 5. Zeolite's impact on slump value

3.5 Gamma-rays Measurements and Calculations

The gamma-ray shielding performance of concrete was evaluated by measuring and calculating the mass attenuation coefficient (μ/ρ, cm^2/g). The experimental measurements showed good agreement with theoretical calculations from the WinXCom computer program (version 3.1), especially in the energy range of 344 - 1407 keV. The primary gamma-ray interaction mechanism in these concretes was identified as Compton scattering, with a lesser contribution from the photoelectric effect at lower energies.

Document Observations:

The document states there is "a good agreement between the measured values of mass attenuation coefficients and that calculated by winXCom computer program (version 3.1), especially in the energy range of 344 - 1407 keV."

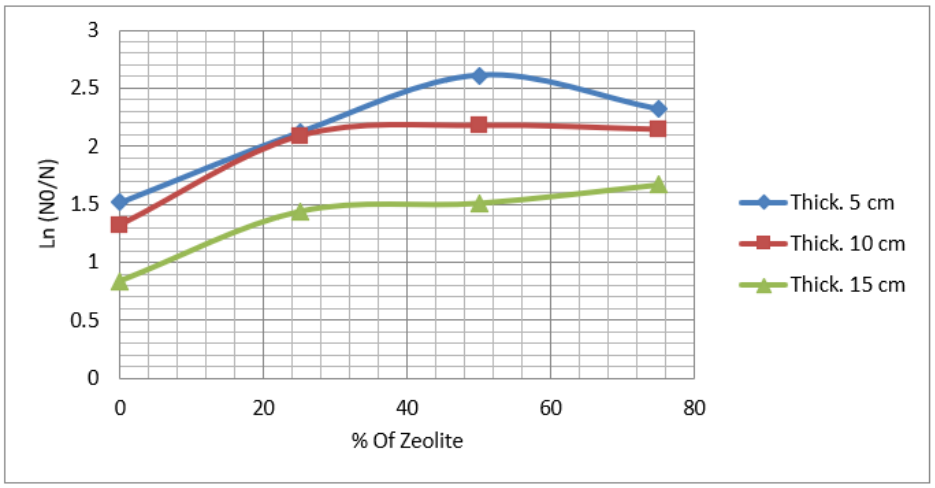

Figure 5. Zeolite's impact on slump value

TABLE 1. Chemical composition of Zeolite

Sample ID - (Z-0%)	
Thich. (t) - cm	5
Diam. (D) - cm	15
GGBFS %	5
Test Duration (sec.)	300
Without Specimens	
Full Energy Peak (Kev)	662
Counts/Seconds Cnts	2876
With Specimens	
Full Energy Peak (Kev)	662
Counts/Seconds Cnts	1245
% of (ɣ - Ray) absorbtion of specimen	56.71
(N0) Counts recorded without absorber - without specimens	2876
(N) Counts recorded with absorber - with specimens	1245
(t)	5
N0/N	2.310
Ln N0/N	0.837265
Linear attenuation coefficient, $\mu = 1/t$ (Ln N0/N)	0.167453

4. Conclusions

Based on the experimental results, the following conclusions could be drawn:

1. Optimal Zeolite Content for Mechanical Performance:
   The mechanical strength of concrete, particularly compressive strength, improves significantly when cement is replaced with zeolite up to 50 wt.%. Beyond this level, the strength begins to decline, but remains above that of the control mix (0% zeolite). This enhancement is attributed to the pozzolanic reaction of zeolite with calcium hydroxide, producing additional calcium-silicate-hydrate (C-S-H) gel, which densifies the microstructure and reduces porosity.
2. Enhanced Corrosion Resistance of Embedded Steel:
   The corrosion resistance of steel reinforcement embedded in zeolite-modified concrete is notably improved up to a 50 wt.% replacement level. Electrochemical measurements (open-circuit potential, potentiodynamic polarization) and optical microscopy confirm that zeolite reduces the corrosion rate by lowering the permeability and chloride ion ingress, thereby protecting the passive layer on the steel surface.
3. Superior Gamma-Ray Attenuation at 50 wt.% Zeolite:
   For gamma-ray shielding, the mass attenuation coefficient (μ/ρ, cm^2/g) is maximized at a zeolite content of 50 wt.% across most investigated energy lines (121.78 – 1407.92 keV). Experimental values show excellent agreement with theoretical calculations performed using the WinXCom computer program (version 3.1). The dominant interaction mechanism is Compton scattering, with a minor contribution from the photoelectric effect at lower energies.
4. Improved Neutron Shielding Characteristics:
   The macroscopic neutron cross-section (Σ, cm^{-1}) of concrete increases with the addition of zeolite, owing to the material's higher hydrogen content and its unique aluminosilicate structure. This makes zeolite-modified concrete an effective barrier for mixed neutron-gamma radiation fields, such as those encountered in nuclear facilities and medical radiotherapy rooms.
5. Sustainable and Multifunctional Construction Material:
   Geopolymerized zeolite concrete offers a sustainable alternative to ordinary Portland cement by reducing greenhouse gas emissions (cement production accounts for 5-7% of global CO_2 emissions). Besides its environmental benefits, zeolite concrete simultaneously provides enhanced mechanical properties, improved durability against corrosion, and superior radiation attenuation, making it a promising candidate for specialized infrastructure (e.g., nuclear power plants, waste storage facilities, and healthcare centers).

Author Contributions: For this research articles with one author, "Conceptualization, Abd Al-Kader A. Al Sayed; methodology, Abd Al-Kader A. Al Sayed.; software, Amr Abdelkhalik.; validation, Abd Al-Kader A. Al Sayed.; formal analysis, Amr Abdelkhalik.; investigation, Abd Al-Kader A. Al Sayed.; resources, Amr Abdelkhalik.; data curation, Amr Abdelkhalik.; writing—original draft preparation, Abd Al-Kader A. Al Sayed.; writing—review and editing, Amr Abdelkhalik.; visualization, Abd Al-Kader A. Al Sayed.; supervision, Amr Abdelkhalik.; project administration, Abd Al-Kader A. Al Sayed.; funding acquisition, Abd Al-Kader A. Al Sayed. Author has read and agreed to the published version of the manuscript."

Funding: This research received no external funding

Data Availability Statement: Data Availability Statement: The original contributions presented in this study are included in the article. Further inquiries can be directed to the corresponding author.

Conflicts of Interest: The authors declare no conflicts of interest.

References

[1] I. O. Akgun, M. Uysal, and M. Yilmaz, "Sustainable geopolymer composites incorporating waste volcanic tuff and recycled geopolymer concrete powder as base materials," *Constr. Build. Mater.*, vol. 509, p. 145161, 2026, doi: https://doi.org/10.1016/j.conbuildmat.2026.145161.

[2] B. Gopalakrishna and D. Pasla, "Development of metakaolin based high strength recycled aggregate geopolymer concrete," *Constr. Build. Mater.*, vol. 391, p. 131810, 2023, doi: https://doi.org/10.1016/j.conbuildmat.2023.131810.

[3] O. H. Ören *et al.*, "Effects of microencapsulated phase change material on physico-mechanical and thermoregulation performance of lightweight geopolymer concrete with zeolite and perlite," *J. Energy Storage*, vol. 109, p. 115225, 2025, doi: https://doi.org/10.1016/j.est.2024.115225.

[4] S. Mani, P. Partheeban, and K. Andiyappan, "Mechanical and durability performance of multilayered hemp–sisal fiber-reinforced geopolymer concrete for sustainable construction," *Structures*, vol. 81, p. 110328, 2025, doi: https://doi.org/10.1016/j.istruc.2025.110328.

[5] A. Mohsen, M. Kohail, A. A. Abadel, Y. R. Alharbi, M. L. Nehdi, and M. Ramadan, "Correlation between porous structure analysis, mechanical efficiency and gamma-ray attenuation power for hydrothermally treated slag-glass waste-based geopolymer," *Case Stud. Constr. Mater.*, vol. 17, p. e01505, 2022, doi: https://doi.org/10.1016/j.cscm.2022.e01505.

[6] C. Karakurt and I. B. Topçu, "Effect of blended cements produced with natural zeolite and industrial by-products on alkali-silica reaction and sulfate resistance of concrete," *Constr. Build. Mater.*, vol. 25, no. 4, pp. 1789–1795, 2011, doi: 10.1016/j.conbuildmat.2010.11.087.

[7] R. Shawabkeh, A. Al-Harahsheh, M. Hami, and A. Khlaifat, "Conversion of oil shale ash into zeolite for cadmium and lead removal from wastewater," *Fuel*, vol. 83, no. 7–8, pp. 981–985, 2004, doi: 10.1016/j.fuel.2003.10.009.

[8] H. M. Al-Jabali, W. F. Edris, S. Khairy, G. N. Mohamed, H. A. Elsayed, and A. A. El-Latief, "Impact of PEG400–Zeolite Performance as a Material for Enhancing Strength of the Mechanical Properties of LECA/Foamed Lightweight Concrete," *Infrastructures*, vol. 9, no. 9, 2024, doi: 10.3390/infrastructures9090149.

[9] H. Jalilifar and F. Sajedi, "Micro-structural analysis of recycled concretes made with recycled coarse concrete aggregates," *Constr. Build. Mater.*, vol. 267, no. January 2021, p. 121041, 2021, doi: 10.1016/j.conbuildmat.2020.121041.

[10] M. J. A. Mijarsh, M. A. Megat Johari, and Z. A. Ahmad, "Effect of delay time and Na2SiO3 concentrations on compressive strength development of geopolymer mortar synthesized from TPOFA," *Constr. Build. Mater.*, vol. 86, pp. 64–74, 2015, doi: 10.1016/j.conbuildmat.2015.03.078.

[11] N. Poornima, D. Katyal, T. Revathi, M. Sivasakthi, and R. Jeyalakshmi, "Effect of curing on mechanical strength and microstructure of fly ash blend GGBS geopolymer, Portland cement mortar and its behavior at elevated temperature," *Mater. Today Proc.*, vol. 47, no. xxxx, pp. 863–870, 2021, doi: 10.1016/j.matpr.2021.04.087.

[12] C. Karakurt and İ. Topçu, "Effect of blended cements produced with natural zeolite and volcanic tuffs on sulfate resistance of concrete," 2009.

[13] A. Fernández-Jiménez and A. Palomo, "Composition and microstructure of alkali activated fly ash binder: Effect of the activator," *Cem. Concr. Res.*, vol. 35, no. 10, pp. 1984–1992, 2005, doi: 10.1016/j.cemconres.2005.03.003.

[14] M. Ding, S. Kelkar, and A. Meijer, "Surface complexation modeling of americium sorption onto volcanic tuff," *J. Environ. Radioact.*, vol. 136, pp. 181–187, 2014, doi: https://doi.org/10.1016/j.jenvrad.2014.06.007.

[15] N. B. Singh and B. Middendorf, "Geopolymers as an alternative to Portland cement: An overview," *Constr. Build. Mater.*, vol. 237, pp. 1–15, 2020, doi: 10.1016/j.conbuildmat.2019.117455.

[16] J. Davidovits, "Properties of Geopolymer Cements," *First Int. Conf. Alkaline Cem. Concr.*, pp. 131–149, 1994.

[17] M. Cyr and R. Pouhet, *Resistance to alkali-aggregate reaction (AAR) of alkali-activated cement-based binders*. Woodhead Publishing Limited, 2015. doi: 10.1533/9781782422884.3.397.

[18] A. Sepulcre-Aguilar and F. Hernández-Olivares, "Assessment of phase formation in lime-based mortars with added metakaolin, Portland cement and sepiolite, for grouting of historic masonry," *Cem. Concr. Res.*, vol. 40, no. 1, pp. 66–76, 2010, doi: 10.1016/j.cemconres.2009.08.028.

[19] A. A. Kader, C. A. Secondary, and C. Author, "International Journal of Concrete Structures and Materials Assessing the Durability of Oil Shale Ash as a Partial OPC Replacement in Mortar : A Study on Mechanical Properties under Sulfate".

[20] M. Criado, A. Palomo, and A. Fernández-Jiménez, "Alkali activation of fly ashes. Part 1: Effect of curing conditions on the carbonation of the reaction products," *Fuel*, vol. 84, no. 16, pp. 2048–2054, 2005, doi: 10.1016/j.fuel.2005.03.030.

[21] H. Yu *et al.*, "Effect of mixing sequence on asphalt mixtures containing waste tire rubber and warm mix surfactants," *J. Clean. Prod.*, vol. 246, pp. 1–35, 2020, doi: 10.1016/j.jclepro.2019.119008.

[22] K. B. Ramkumar, P. R. Kannan Rajkumar, S. Noor Ahmmad, and M. Jegan, "A Review on Performance of Self-Compacting Concrete – Use of Mineral Admixtures and Steel Fibres with Artificial Neural Network Application," *Constr. Build. Mater.*, vol. 261, p. 120215, 2020, doi: 10.1016/j.conbuildmat.2020.120215.